

# Diagnosing breast cancer using diffuse reflectance spectroscopy and intrinsic fluorescence spectroscopy

**Zoya Volynskaya**

**Abigail S. Haka**

**Kate L. Bechtel**

Massachusetts Institute of Technology  
Laser Biomedical Research Center  
G. R. Harrison Spectroscopy Laboratory  
77 Massachusetts Avenue, 6-218M  
Cambridge, Massachusetts 02139

**Maryann Fitzmaurice**

**Robert Shenk**

**Nancy Wang**

University Hospitals–Case Medical Center  
and  
Case Western Reserve University  
Cleveland, Ohio 44106

**Jon Nazemi**

**Ramachandra R. Dasari**

**Michael S. Feld**

Massachusetts Institute of Technology  
Laser Biomedical Research Center  
G. R. Harrison Spectroscopy Laboratory  
77 Massachusetts Avenue, 6-218M  
Cambridge, Massachusetts 02139

**Abstract.** Using diffuse reflectance spectroscopy and intrinsic fluorescence spectroscopy, we have developed an algorithm that successfully classifies normal breast tissue, fibrocystic change, fibroadenoma, and infiltrating ductal carcinoma in terms of physically meaningful parameters. We acquire 202 spectra from 104 sites in freshly excised breast biopsies from 17 patients within 30 min of surgical excision. The broadband diffuse reflectance and fluorescence spectra are collected via a portable clinical spectrometer and specially designed optical fiber probe. The diffuse reflectance spectra are fit using modified diffusion theory to extract absorption and scattering tissue parameters. Intrinsic fluorescence spectra are extracted from the combined fluorescence and diffuse reflectance spectra and analyzed using multivariate curve resolution. Spectroscopy results are compared to pathology diagnoses, and diagnostic algorithms are developed based on parameters obtained via logistic regression with cross-validation. The sensitivity, specificity, positive predictive value, negative predictive value, and overall diagnostic accuracy (total efficiency) of the algorithm are 100, 96, 69, 100, and 91%, respectively. All invasive breast cancer specimens are correctly diagnosed. The combination of diffuse reflectance spectroscopy and intrinsic fluorescence spectroscopy yields promising results for discrimination of breast cancer from benign breast lesions and warrants a prospective clinical study. © 2008 Society of Photo-Optical Instrumentation Engineers. [DOI: 10.1117/1.2909672]

Keywords: cancer; breast; diagnosis; reflectance; fluorescence; spectroscopy.

Paper 07381R received Sep. 14, 2007; revised manuscript received Dec. 11, 2007; accepted for publication Dec. 12, 2007; published online Apr. 30, 2008.

## 1 Introduction

Screening procedures such as x-ray mammography, ultrasound, and/or palpation are the first step in diagnosing breast cancer. Screening procedures do not accurately identify malignant tissue. Therefore, to establish a diagnosis, the patient must undergo breast biopsy followed by histopathological diagnosis. Due to the lack of specificity of mammography, a high percentage of suspected abnormal lesions (70 to 90%) are found to be benign or normal upon biopsy,<sup>1</sup> resulting in unnecessary cost, patient trauma, and time delay to obtain histopathological diagnosis. Imaging and spectroscopic optical diagnostic techniques are currently being explored to reduce the number of unnecessary breast biopsies in a minimally invasive manner.

Diffuse optical tomography (DOT), an optical imaging technique to identify suspect lesions, is currently under study.<sup>2</sup> Similar to current screening techniques, it is noninvasive and can detect lesions deep within the breast. It employs light of a number of near-IR wavelengths. Contrast, provided by scattering and absorption, measures relative concentrations of oxy- and deoxyhemoglobin, as well as the presence of lipids

and water content.<sup>3</sup> However, this technique has a low resolution,<sup>4,5</sup> due to which lesions of small size go undetected; a resolution of 4 to 13 mm has been reported, and the sources of contrast are limited.<sup>3,2,6</sup> Despite these challenges, DOT has been utilized in several reported breast cancer studies.<sup>7,8</sup>

A number of promising optical spectroscopy techniques for diagnosing breast cancer are also under study. These techniques currently employ point contact probes, but have the potential to be extended to imaging modes.<sup>9</sup> The most frequently utilized methods are diffuse reflectance spectroscopy<sup>10–12</sup> (DRS) and fluorescence spectroscopy.<sup>13–15</sup> As of now, intrinsic fluorescence spectroscopy<sup>16</sup> (IFS), a technique that uses diffuse reflectance to suppress the effects of scattering and absorption in fluorescence, has not been implemented. The objective of this study is to explore the use of DRS and IFS, in combination, to identify and diagnose suspect lesions.

Briefly, DRS measures tissue scattering and absorption properties, which provide information about the morphology and biochemistry of the breast tissue epithelium and stroma. DRS typically utilizes broadband UV-visible excitation in the wavelength range 300 to 800 nm, spanning the prominent hemoglobin absorption features. Fluorescence spectroscopy pro-

---

Address all correspondence to Zoya Volynskaya, MS, Laser Biomedical Research Center, G.R. Harrison Spectroscopy Laboratory, Massachusetts Institute of Technology, 77 Massachusetts Ave, 6-218M, Cambridge, MA 02139; Tel: (617) 253-5077; Fax: (617) 253-4513; E-mail: zivolyns@mit.edu

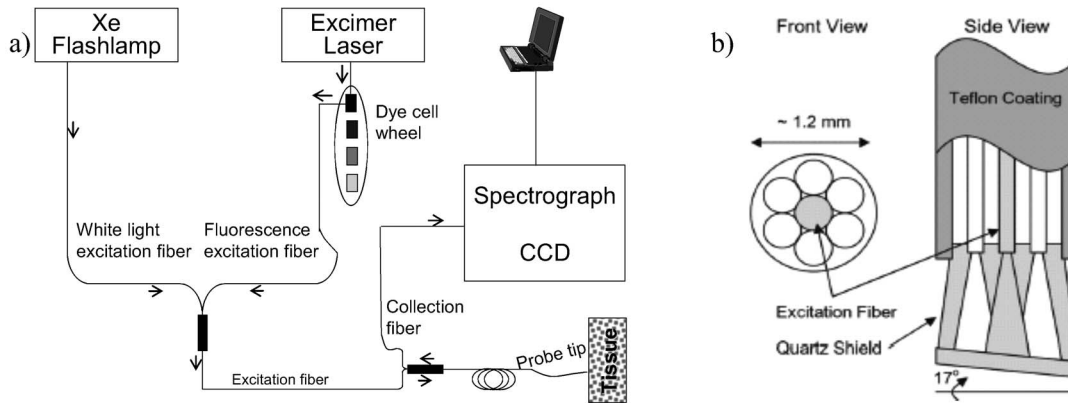


**Fig. 1** (a) FastEEM clinical spectrophotometer and (b) schematic diagram of the distal tip of the optical fiber probe.

vides information about the endogenous tissue fluorophores excited with UV-visible light in the same wavelength range 300 to 800 nm. Fluorophores excited in this range have the most diagnostic significance. However, fluorescence spectra recorded from tissue are distorted by absorption and scattering, thereby limiting the accuracy of the extracted information. To overcome this problem, DRS can be used in conjunction with the measured fluorescence spectrum to extract the intrinsic (undistorted) fluorescence.<sup>17,16</sup> This process is called intrinsic fluorescence spectroscopy (IFS).

The DRS and fluorescence studies published up to now have focused on differentiating malignant from nonmalignant tissues. However, it is also clinically important to discriminate benign lesions that may carry a risk of breast cancer or that need to be surgically excised from normal breast tissue. For example, fibrocystic change is a benign condition that does not require excision, whereas fibroadenoma proliferates rapidly and must be excised. As our data will show, DRS and fluorescence spectroscopy have the potential to identify these lesions in real time at the bedside when performed percutaneously using a fiber optic probe inserted through a breast biopsy needle.

Furthermore, previously used diagnostic algorithms have not been based on parameters that can be identified as pathophysiological features of disease. While doing so is not a requirement for success, the use of parameters that may be directly compared to histopathology is likely to lead to more robust algorithms and to aid clinicians in interpreting spectroscopic results. It also represents a step toward quantifiable, objective tissue diagnosis, as compared to subjective histopathology analysis.

We report an *ex vivo* spectroscopic study of freshly excised human breast tissue. We use DRS and fluorescence, combined in a particular manner, to discriminate breast cancer from both benign breast lesions and normal breast tissue. Our technique, which we refer to subsequently as DRS-IFS, provides a more complete biochemical, morphological, and metabolic tissue profile than either modality alone. Our analysis extracts parameters that optimize classification and, at the same time, provide physical insight. This added information should enable the development of a more robust diagnostic algorithm.

## 2 Instrumentation

A clinical instrument for DRS-IFS studies, the FastEEM [Fig. 1(a)], was developed at the G.R. Harrison Spectroscopy Laboratory at the Massachusetts Institute of Technology<sup>18</sup> (MIT). This instrument collects white light reflectance and fluorescence excitation-emission matrices (EEMs) in a fraction of a second. It delivers a sequence of 10 excitation laser pulses (308 to 480 nm) and two white light pulses (300 to 800 nm) to the tissue via an optical fiber probe, which is in the form of a flexible catheter with an overall length of 3 m and a diameter of approximately 1.2 mm [Fig. 1(b)]. The distal tip consists of a single delivery fiber surrounded by six collection fibers, all with core diameters of 200  $\mu\text{m}$ , and terminated with a transparent, protective optical shield.<sup>18</sup> The tip is brought into gentle contact with the tissue when data are taken. The diameter of tissue sampled is approximately 600  $\mu\text{m}$ , with depth sensing of approximately 100  $\mu\text{m}$ . The same probe delivers the excitation light and collects the diffusely reflected white light and fluorescence. At the proximal end of the probe, the collection fibers are confined in a single line and imaged onto the slit of an intensified CCD detector. Ten laser-induced fluorescence emission spectra and the two white light reflectance spectra are collected in approximately 0.3 s. Sufficient SNR is obtained by averaging five measurements, resulting in a typical acquisition time of 1.5 s. The SNR, determined as the ratio of the peak of the signal to the standard deviation of the noise, was found to be 100.

The instrument was calibrated daily prior to data collection. Calibration consisted of four steps: (1) a background spectrum of water was collected and subtracted from all subsequent measurements to correct for dark current and stray light; (2) the excitation intensities at each of 10 wavelengths were then normalized by measuring a rhodamine B dye mixture; (3) a Spectralon standard with 20% reflectance was then measured to account for the wavelength-dependent system response; (4) and finally, a mercury spectrum was acquired to calibrate wavelength.

## 3 Patients and Breast Tissue Handling

This *ex vivo* study was conducted at the University Hospitals-Case Medical Center (UHC) under approval from the UHC

Institutional Review Board and the MIT Committee on the Use of Humans as Experimental Subjects. Spectra were collected from fresh breast surgical specimens within 30 min after excisional biopsy ( $n=16$ ) and partial mastectomy (lumpectomy;  $n=1$ ) procedures. Overall, we have obtained 202 spectra from 104 sites, providing approximately 2 spectra per site. Most of the 30-min delay was due to gross examination, inking, and sectioning of the specimen performed as part of the routine pathology intraoperative consultation. For each surgical specimen examined, data were collected from multiple tissue sites of interest identified by the pathologist. Spectra were also acquired from the colloidal inks used to mark the surgical margins of each specimen, and it was confirmed that no artifacts were introduced in the data as a result of this processing step.

Some of the data collected were subsequently excluded from the analysis. Specifically, DRS data with overall reflectance of less than 1% were excluded because of the inability to use reflectance information of that data to process the fluorescence data to obtain the intrinsic fluorescence. Sites whose spectra failed this criterion (11 sites) were found to be contaminated by the presence of surface blood that absorbed too much of the reflected light. Additionally, specimens from patients with preoperative chemotherapy or who underwent repeat excisional biopsy were excluded from analysis (7 specimens). Sites exhibiting other lesions [ductal epithelial hyperplasia,  $n=2$ ; fat necrosis,  $n=1$ ; and ductal carcinoma *in situ* (DCIS),  $n=6$ ] were also excluded, as their limited numbers precluded development of a robust diagnostic algorithm. Following these exclusions, 202 IFS and DRS spectra acquired from a total of 104 breast tissue sites (1 and often 2 spectra per site) in specimens from 17 consecutive patients remained and were used for further analysis.

After acquisition of the spectra, the exact site of probe placement was marked with colloidal ink for registration with histopathology. The breast specimens were then fixed in formalin and submitted for routine pathology evaluation, performed by an experienced breast pathologist blinded to the spectroscopy results. The histopathology diagnoses were<sup>19</sup> 31 normal, 55 fibrocystic change, 9 fibroadenoma, and 9 invasive carcinoma (all infiltrating ductal carcinoma). The relative number of each diagnosis in this data set closely resembles the typical prevalence for diseases of breast tissue.<sup>1</sup>

#### 4 Data Analysis

We analyzed the DRS spectrum from each breast tissue site using a mathematical model based on the diffusion approximation of light propagation in tissue to determine the values of the absorption coefficient  $\mu_a(\lambda)$  and the reduced scattering coefficient  $\mu'_s(\lambda)$ , previously described in detail.<sup>17</sup> The model requires index of refraction  $n$ , which for soft biological tissue has a typical value<sup>20</sup> of 1.35 to 1.45. Two absorbers, oxyhemoglobin and  $\beta$ -carotene,<sup>21</sup> were used to model the extracted absorption coefficient  $\mu_a$ . During our study, the tissue was exposed to room air and hemoglobin was oxygenated; therefore, deoxyhemoglobin was not included. For the reduced scattering coefficient  $\mu'_s(\lambda)$ , wavelength dependence of the form  $A\lambda^{-B}$  was employed.<sup>22</sup>

IFS spectra were extracted from the combined fluorescence and DRS spectra, as previously described.<sup>23</sup> An IFS spectrum

**Table 1** Expected fluorophores for various excitation wavelengths.

	Excitation Wavelength (nm)			
	308	340	360	425
<b>Fluorophores</b>	NADH	NADH <sup>a</sup>	NADH	collagen
	collagen	collagen <sup>a</sup>	collagen	elastin <sup>a</sup>
	Tryptophan <sup>a</sup>	elastin	FAD	FAD <sup>a</sup>
			porphyrins <sup>a</sup>	

<sup>a</sup>Optimal excitation wavelength for each fluorophore.

is composed of a linear combination of the spectra of the individual fluorophores present in the tissue. However, differences in local chemical environments, such as in tissue, may alter the shape of a fluorophore spectrum from that of its pure component.<sup>24</sup> Therefore, pure component spectra were not directly fit to a given IFS spectrum. Instead, the IFS spectra were analyzed using multivariate curve resolution (MCR) with nonnegativity constraints, a standard chemometric method.<sup>25</sup> MCR generates spectral components by adjusting the spectral shape of initial input parameters to minimize the fitting error to a given tissue spectrum. The initial input spectra in our case were the pure component spectra of fluorophores known to be present in breast tissue<sup>24</sup> (Table 1). The maximum number of the initial input spectra was not constrained; however, on analysis, it was found that only two spectra were required to produce good fits to the data. The resulting MCR-generated spectral components at 340 nm are shown in Figs. 2(a) and 2(b). The combined basis spectra and fit to a representative IFS spectrum are shown in Fig. 2(c). The MCR-generated spectral components are similar to the spectra of NADH and collagen-like, respectively, but are broader and red-shifted, as expected of fluorophores in a tissue environment.<sup>26</sup>

As stated previously, the FastEEM instrument provides emission spectra at 10 different excitation wavelengths. Collagen, NADH, elastin, tryptophan, FAD, and porphyrins, the native fluorophores of breast tissue, have their maximum emission at 308, 340, 360, and 425 nm excitation wavelengths<sup>26</sup> (Table 1). Thus, those four fluorescence excitation wavelengths were employed in the initial analysis. However, it was found that not all of these fluorophores could be detected, presumably because they were not present in our specimens at high enough levels. These include elastin excited at 340 nm and FAD and porphyrins excited at 360 nm. The absence of these fluorophores was confirmed by attempting to extract their basis spectra using MCR and finding that the contributions were negligible.

Of the measured fluorophores, only NADH and collagen-like excited at 340 and 360 nm were required to obtain good fits to the IFS spectra. However, no substantial differences in the fluorophore contributions at those two wavelengths were observed. Due to the proximity in wavelength of 340 and 360 nm, the difference in the penetration depth of the light ( $<5 \mu\text{m}$ ) evidently was not sufficient to reveal these differences. Averaging the information at these two wavelengths

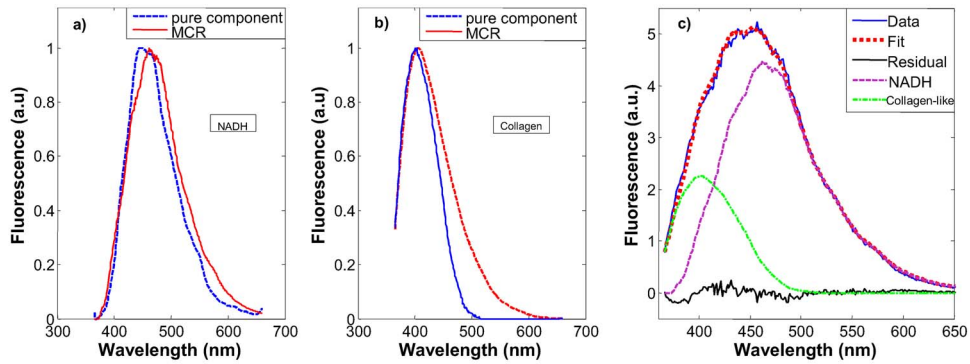


**Fig. 2** (a) and (b) Comparison of pure component spectra (blue, dashed lines) and MCR basis spectra (red solid lines) excited at 340 nm for (a) NADH and (b) collagen; (c) representative spectrum fit with a linear combination of NADH (magenta, dotted line) and collagen-like basis spectra (green, dash-dotted line) [data (blue, solid line); fit (red, dotted line); residual (black)]. (Color online only)

did not improve the fits. To reduce complexity, we opted to utilize only one excitation wavelength, with the added benefit that as a result only one UV source will be required in future clinical instruments. Therefore, contributions of NADH and collagen-like excited at 340 nm were chosen for algorithm

development, as this is the wavelength for maximum emission of NADH. Representative DRS and IFS spectra collected with 340-nm excitation are shown in Fig. 3.

Thus, the data analysis of each tissue site was performed using two spectra (one DRS and one IFS). Spectra were fur-

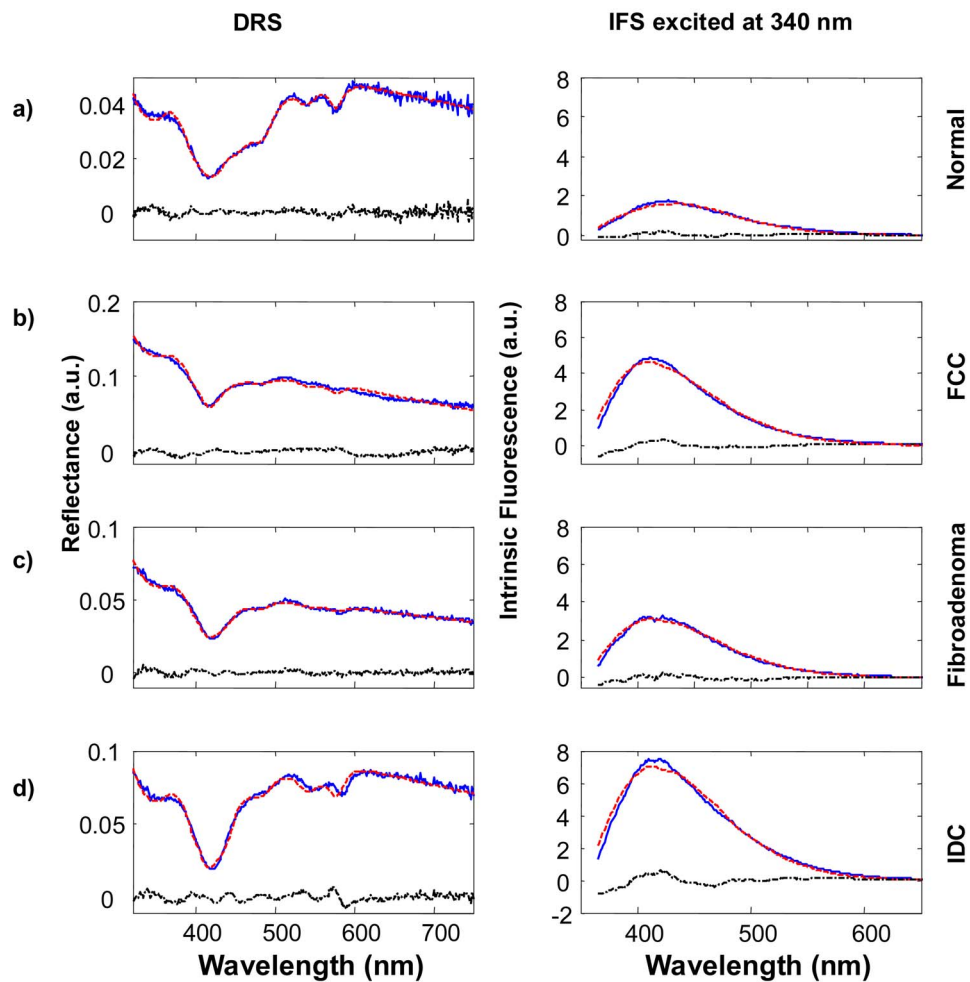


**Fig. 3** Representative spectra of DRS and IFS excited at 340 nm for all pathologies: (a) normal tissue, (b) fibrocystic change lesion, (c) fibroadenoma lesion, and (d) infiltrating ductal carcinoma lesion [data (blue, solid line); fit (red, dashed line); residual (black, dash-dotted line)]. (Color online only)



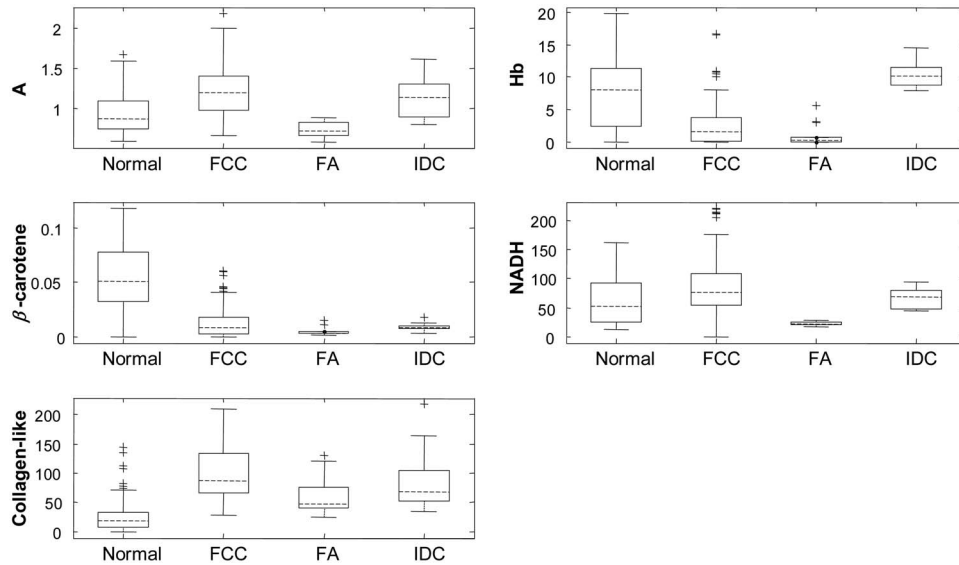


**Fig. 4** Boxplots of normal tissue (Normal), fibrocystic change (FCC), fibroadenoma (FA), and infiltrating ductal carcinoma (IDC) for diagnostically relevant parameters: *A*, scattering parameter extracted from DRS; Hb (oxyhemoglobin) and  $\beta$ -carotene, absorption fit coefficients extracted from DRS; and NADH and collagen-like, fit coefficients from IFS spectra excited at 340 nm.

ther characterized by six parameters: *A* and *B*—scattering parameters, fit coefficients of oxyhemoglobin and  $\beta$ -carotene, as well as the fit coefficients of collagen-like and NADH.

### 5 Algorithm Development

Following data analysis, all of the fit parameters, except *B*, were found to be diagnostically relevant. Boxplots for these parameters are shown in Fig. 4. (A boxplot is a graphical representation of data spread, with the first, second, and third quartiles “contained” in the box; the median for the data set is indicated by the black center line. The interquartile range is defined as the distance between the first and third quartiles. The extreme values are defined as 1.5 times the interquartile range, measured from the median. Data points outside of this range, indicated by crosses, are defined as outliers.) This form of data depiction is useful for visually examining the diagnostic capability of each parameter. For example, the boxplot for collagen-like indicates that normal breast sites may be partially separated from other sites using this parameter. Note that diagnostic parameters in a particular tissue type may be correlated. Hence, one parameter may provide only partial separation, but the use of a second parameter in combination with it may provide full separation. Visualizing this behavior requires a 2-D scatter plot and is not revealed by the boxplots.

The desired algorithm must be able to classify invasive breast cancer (in this case, infiltrating ductal carcinoma), benign breast lesions such as fibroadenoma and fibrocystic change, and normal breast tissue. Because each of these tissue types can likely be characterized using different diagnostic parameters, we performed the analysis in a stepwise fashion, as shown in Fig. 5. Initially, normal specimens are separated from the rest of the specimens (step 1), followed by the separation of fibroadenoma from fibrocystic change and infiltrating ductal carcinoma (step 2), and finally, the separation of infiltrating ductal carcinoma from fibrocystic change lesions (step 3). The diagnostic algorithm was developed using logis-

tic regression and leave-one-out cross-validation. Histopathology diagnoses were used as the standard against which the spectroscopic diagnoses were compared. By maximizing the sensitivity of each stage of the algorithm we were able to identify the diagnostic parameters that can best discriminate pathologies of breast tissue.

The scatter plots and decision lines for each step of the diagnostic algorithm are depicted in Fig. 6. In step 1, normal sites are classified using the collagen-like and  $\beta$ -carotene fit coefficients extracted from IFS at 340-nm excitation and DRS, respectively [Fig. 6(a)]. In step 2, fibroadenoma sites are discriminated from fibrocystic change and infiltrating ductal carcinoma using the DRS scattering parameter *A* and the IFS NADH fit coefficient [Fig. 6(b)]. Finally, in step 3, infiltrating ductal carcinoma sites are distinguished from fibrocystic change using the DRS oxyhemoglobin and a weaker dependence of IFS collagen-like (excited at 340 nm) fit coefficients [Fig. 6(c)].

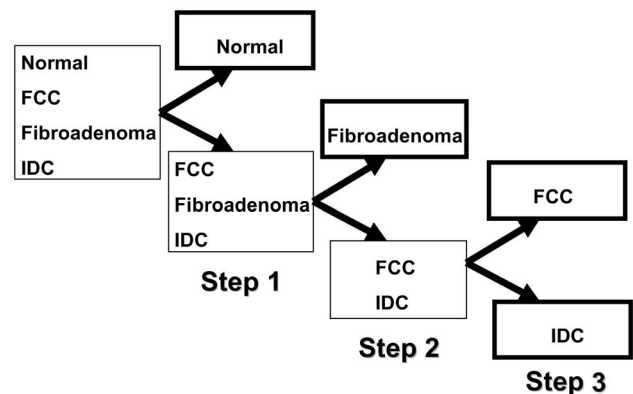


**Fig. 5** Stepwise diagnostic algorithm.

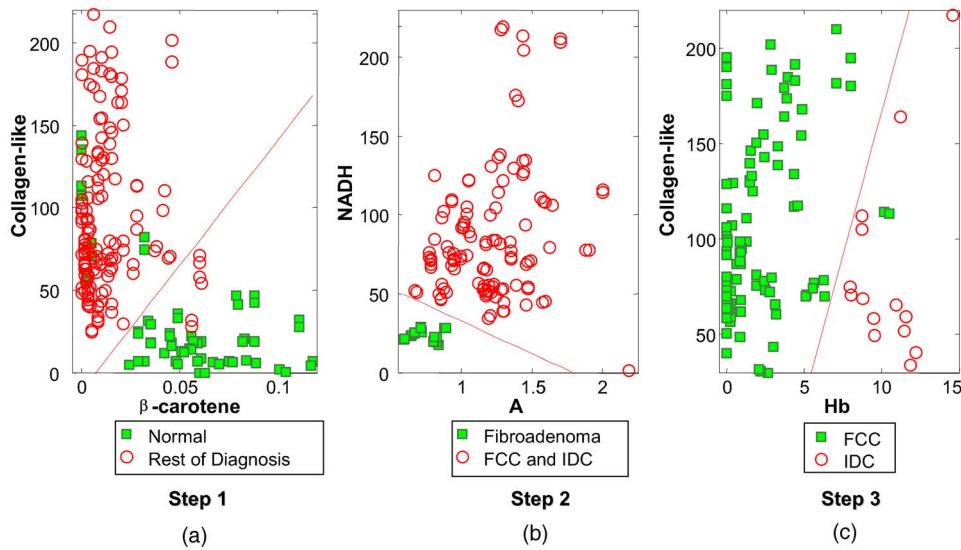


Fig. 6 Discrimination of pathologies using the stepwise algorithm. The three steps are indicated.

### 6 Results and Discussion

Table 2 compares the DRS-IFS spectral diagnoses and the histopathology diagnoses. The diagnostic algorithm achieves the goal of distinguishing normal breast, fibrocystic change, fibroadenoma, and infiltrating ductal carcinoma using physically meaningful parameters extracted from DRS and IFS. All of the invasive carcinomas are correctly classified and only three normal specimens and one fibrocystic change lesion are misclassified as infiltrating ductal carcinoma. The total efficiency (overall accuracy) is 91% (95/104). The sensitivity and specificity are 100 and 96%, respectively, with sensitivity defined as the fraction of cancers correctly identified by the algorithm, and specificity defined as the fraction of correctly identified noncancerous lesions. The positive and negative predictive values are 69 and 100%, respectively. The positive predictive value (PPV) is the probability that a positive result is accurate, i.e., that the patient actually has the specified disease. The negative predictive value (NPV) is the probability that a negative result is accurate.<sup>27</sup> NPV is the most important value for the clinical test we envision because it is less adverse to the health of a patient to excise normal or benign lesions (owing to a low PPV for a given technique) than to leave a cancerous lesion in place (owing to a low NPV).

Therefore, it is important that a technique have a high NPV to be effective in clinical practice. Note that, unlike sensitivity and specificity, predictive values depend on the characteristics of the population and, in particular, the prevalence of disease. In our study, the disease prevalence of the data set is similar to the usual prevalence encountered in breast cancer; predictive values achieved by our technique are thus meaningful.

Our use of multiple parameters from multiple spectroscopic modalities enables discrimination of benign lesions from normal and malignant tissues. Furthermore, it allows for discrimination among different types of benign lesions in the majority of cases. This is difficult to accomplish using only one or two parameters. Gupta et al. utilized differences in the integrated fluorescence intensities to separately discriminate cancerous from fibroadenoma and cancerous from normal tissue types in an *ex vivo* study. They were unsuccessful in their attempt to discriminate fibroadenoma from normal tissue owing to similar fluorescence intensities.<sup>14</sup> Palmer et al. examined both fluorescence and diffuse reflectance spectroscopy during an *ex vivo* study.<sup>28</sup> Their study utilized principal component analysis followed by a support vector machine to discern differences in spectral components of the pathology groupings. It was found that multiexcitation fluorescence

Table 2 Comparison of DRS-IFS and histopathologic classifications, where DRS-IFS diagnostic algorithm has an overall accuracy of 91% (95/104).

DRS-IFS	Pathology			
	Normal (31 Samples)	Fibrocystic Change (55 Samples)	Fibroadenoma (9 Samples)	Infiltrating Ductal Carcinoma (9 Samples)
Normal	26	3	0	0
Fibrocystic change	2	51	0	0
Fibroadenoma	0	0	9	0
Infiltrating ductal carcinoma	3	1	0	9

**Table 3** Synopsis of previous works that utilizes DRS and/or fluorescence spectroscopy to diagnose breast cancer and reports sensitivity (Se) and specificity (Sp) values.

Technique	Study	Se (%)	Sp (%)	Patient (number)	Site (number)	Discrimination	Reference
DRS	<i>In vivo</i>	69	85	31	126	Malignant versus nonmalignant	Bigio et al. <sup>10a</sup>
	<i>Ex vivo</i>	83	76	45	97	Malignant versus nonmalignant	Zhu et al. <sup>12a</sup>
	<i>Ex vivo</i>	30	78	32	56	Malignant versus nonmalignant	Palmer et al. <sup>28a</sup>
	<i>Ex vivo</i>	100	100	17	104	Normal, FCC, fibroadenoma, IDC	Volynskaya, 2008
Fluorescence	<i>Ex vivo</i>	99.6	98.4	63	911	IDC versus fibroadenoma	Gupta et al. <sup>14a</sup>
		98.8	98.7			IDC versus normal	
	<i>Ex vivo</i>	70	92	32	56	Malignant versus nonmalignant	Palmer et al. <sup>28a</sup>
Intrinsic fluorescence	<i>Ex vivo</i>	89	66	17	104	Normal, FCC, fibroadenoma, IDC	Volynskaya, 2008
DRS and fluorescence	<i>Ex vivo</i>	70	91.7	32	56	Malignant versus nonmalignant	Breslin et al. <sup>11a</sup>
DRS and intrinsic fluorescence	<i>Ex vivo</i>	100	96	17	104	Normal, FCC, fibroadenoma, IDC	Volynskaya, 2008

<sup>a</sup>PPV, NPV, and total efficiency were not reported.

spectroscopy was successful at discriminating malignant and nonmalignant tissues with a sensitivity and specificity of 70 and 92%, respectively. However, the sensitivity (30%) and specificity (78%) of diffuse reflectance spectroscopy alone were significantly lower. They found that the combination of fluorescence and diffuse reflectance spectroscopy did not improve the classification accuracy of an algorithm based on fluorescence spectra alone. Breslin et al.<sup>11</sup> also explored the combination of fluorescence and diffuse reflectance spectroscopy in an *ex vivo* study. Using principle component analysis to discriminate malignant from nonmalignant tissue, they were unable to improve sensitivity and specificity with the combination of techniques from that achieved using only fluorescence spectroscopy. Table 3 provides a synopsis of published results for the application of DRS and fluorescence modalities to the study of breast cancer.

In contrast to these studies, we find that the majority of our diagnostic accuracy in discriminating benign from malignant lesions arises from parameters extracted from DRS. For example, generating a classification scheme from DRS parameters alone (scattering coefficient *A* and relative contributions of  $\beta$ -carotene and oxyhemoglobin), provides a sensitivity, specificity, PPV, NPV, and total efficiencies of 100, 100, 100, 100, and 81% (85/104), respectively. That is, all sites are correctly diagnosed as either benign or malignant. However, benign sites may be misclassified. A total of six normal and one fibroadenomas are misclassified as fibrocystic change, eight fibrocystic change lesions are misclassified as normal, and four fibrocystic change lesions are misclassified as fibroadenoma.

Somewhat surprisingly, an accurate classification scheme could not be generated from IFS parameters alone (relative contributions of NADH and collagen-like). Results for the sensitivity, specificity, PPV, NPV and total efficiency are 89, 66, 20, 98, and 80%, respectively. Note that although the inclusion of IFS parameters into the combined algorithm does

not improve the classification of benign versus malignant lesions, IFS significantly improves the total efficiency (increase of 12% from the DRS algorithm alone). The total efficiency is the only metric that considers the accuracy of the technique in subclassifying the benign lesions; specifically: normal, fibrocystic change, and fibroadenoma.

Although it is difficult to compare and contrast past studies with this current study given the wide range of experimental variables, differences in analysis methods, and differences in classification schemes and scope, we hypothesize that our model-based approach is the key advantage. We correct the observed fluorescence spectra using DRS and extract parameters that represent NADH and collagen-like fluorescence signatures. We also fit the DRS spectra to extract multiple physiological parameters. Further, our analysis better accounts for physical changes in tissue composition that contribute to changes in histopathology. Normal breast tissue consists mostly of adipocytes (fat), whereas most breast lesions are characterized by an increase in fibrous stroma and, as a result, an increase in the amount of collagen.<sup>1</sup> Therefore, in the first stage of our diagnostic algorithm, we expect that normal tissue can be separated from the three types of breast lesions by the relative contributions of collagen-like and  $\beta$ -carotene, a lipid-soluble marker of adipocytes. In the second stage of the algorithm, fibroadenoma is separated from fibrocystic change and infiltrating ductal carcinoma with the aid of NADH and the scattering parameter *A*. By histopathology, fibrocystic change and infiltrating ductal carcinoma are both cellular proliferative lesions, accounting for their relatively large contributions of NADH, a product of cellular metabolism. The parameter *A* is representative of the density of scatterers in the tissue.<sup>17</sup> We expect infiltrating ductal carcinoma to have a relatively high value of the parameter *A*, as a result of fragmentation and disorganization of the collagen fibers in the stroma of invasive cancers due to the action of matrix

metalloproteinases.<sup>29</sup> Finally, in the third stage of the algorithm, infiltrating ductal carcinoma is separated from fibrocystic change on the basis of collagen-like and oxyhemoglobin fit coefficients. As most malignant tumors, including infiltrating ductal carcinoma, are characterized by angiogenesis<sup>1</sup> (increased vasculature), it is not surprising that oxyhemoglobin is useful in separating infiltrating carcinoma from its benign counterpart, fibrocystic change. Interestingly, oxyhemoglobin is also a diagnostic parameter in diffuse optical tomography imaging of breast cancer. It is not as clear why collagen-like is useful in distinguishing infiltrating ductal carcinoma from fibrocystic disease, as both demonstrate stromal fibrosis. However, since there are differences in the types of collagen present in the stroma of these two lesions,<sup>30</sup> it is possible that the MCR collagen-like basis spectrum better reflects the type of collagen present in fibrocystic change.

The number of DCIS specimens is too small to develop a diagnostic algorithm. A larger clinical study is required to identify DCIS using our technique.

## 7 Conclusion

We demonstrated the potential of DRS-IFS as a clinical tool for breast cancer diagnosis. Our study is the first to show a marked benefit from the combined use of diffuse reflectance and fluorescence modalities. Our diagnostic algorithm is based on physically meaningful parameters, which include the scattering parameter  $A$ , the absorption of  $\beta$ -carotene and oxyhemoglobin, and the fluorescence of NADH and collagen-like excited at 340 nm, extracted from their spectra using a mathematical model based on the diffusion approximation of light propagation in tissue and multivariate curve resolution. Logistic regression and a leave-one-out cross-validation scheme were employed to determine the optimal diagnostic algorithm. The algorithm resulted in 100% sensitivity, 96% specificity, 69% positive predictive value, 100% negative predictive value and 91% total efficiency. These results are promising, and further study is warranted. As an important next step, our diagnostic algorithm should be prospectively tested in an *ex vivo* or *in vivo* independent clinical study with a larger number of patients. As our diagnostic algorithm was constructed using an *ex vivo* data set that closely reflects disease prevalence, we expect the performance of the algorithm to remain high in a larger study.

Recent work from our group in the application of Raman spectroscopy, a type of vibrational spectroscopy with chemical specificity, to breast cancer diagnosis demonstrates comparable results to the present DRS-IFS study.<sup>31</sup> By combining Raman spectroscopy with DRS-IFS, a multidimensional algorithm capable of discriminating an even broader range of breast lesions may be possible. In addition, other routinely encountered diagnoses, particularly ductal carcinoma *in situ*, should be included in future diagnostic algorithms. This may be accomplished by incorporating parameters from additional techniques, such as Raman spectroscopy.

## Acknowledgments

This study was supported by National Center for Research Resources program Grant No. P41-RR-02594 and the Pathology Associates of University Hospitals.

## References

1. R. Cotran, V. Kumar, and T. Collins, *Robbins Pathologic Basis of Disease*, Philadelphia (1999).
2. J. C. Hebden, H. Veenstra, H. Dehghani, E. M. Hillman, M. Schweiger, S. R. Arridge, and D. T. Delpy, "Three-dimensional time-resolved optical tomography of a conical breast phantom," *Appl. Opt.* **40**(19), 3278–3287 (2001).
3. M. Guven, B. Yazici, X. Intes, and B. Chance, "Diffuse optical tomography with a priori anatomical information," *Phys. Med. Biol.* **50**(12), 2837–2858 (2005).
4. J. Culver, V. Ntziachristos, M. Holboke and A. Yodh, "Optimization of optode arrangement for diffuse optical tomography: a singular-value analysis," *Opt. Lett.* **26**, 701–703 (2001).
5. B. W. Pogue, T. O. McBride, J. Prewitt, U. L. Osterberg, and K. D. Paulsen, "Spatially variant regularization improves diffuse optical tomography," *Appl. Opt.* **38**(13), 2950–2961 (1999).
6. V. Quaresima, S. J. Matcher, and M. Ferrari, "Identification and quantification of intrinsic optical contrast for near-infrared mammography," *Photochem. Photobiol.* **67**(1), 4–14 (1998).
7. X. Cheng, J. M. Mao, R. Bush, D. B. Kopans, R. H. Moore, and M. Chortlon, "Breast cancer detection by mapping hemoglobin concentration and oxygen saturation," *Appl. Opt.* **42**(31), 6412–6421 (2003).
8. G. Boverman, E. L. Miller, A. Li, Q. Zhang, T. Chaves, D. H. Brooks, and D. A. Boas, "Quantitative spectroscopic diffuse optical tomography of the breast guided by imperfect a priori structural information," *Phys. Med. Biol.* **50**(17), 3941–3956 (2005).
9. C. Yu, C. Lau, J. Mirkovic, S. A. McGee, G. O'Donoghue, K. Badizadegan, R. R. Dasari, and M. S. Feld, "Tri-modal spectroscopy imaging," in *Proc. Engineering Conferences, Int.—Advances in Optics for Biotechnology, Medicine and Surgery*, pp., Naples, FL (2007).
10. I. J. Bigio, S. G. Bown, G. Briggs, C. Kelley, S. Lakhani, D. Pickard, P. M. Ripley, I. G. Rose, and C. Saunders, "Diagnosis of breast cancer using elastic-scattering spectroscopy: preliminary clinical results," *J. Biomed. Opt.* **5**(2), 221–228 (2000).
11. T. M. Breslin, F. Xu, G. M. Palmer, C. Zhu, K. W. Gilchrist, and N. Ramanujam, "Autofluorescence and diffuse reflectance properties of malignant and benign breast tissues," *Ann. Surg. Oncol.* **11**(1), 65–70 (2004).
12. C. Zhu, G. M. Palmer, T. M. Breslin, J. Harter, and N. Ramanujam, "Diagnosis of breast cancer using diffuse reflectance spectroscopy: comparison of a Monte Carlo versus partial least squares analysis based feature extraction technique," *Lasers Surg. Med.* **38**(7), 714–724 (2006).
13. G. M. Palmer, C. Zhu, T. M. Breslin, F. Xu, K. W. Gilchrist, and N. Ramanujam, "Monte Carlo-based inverse model for calculating tissue optical properties. Part II: Application to breast cancer diagnosis," *Appl. Opt.* **45**(5), 1072–1078 (2006).
14. P. K. Gupta, S. K. Majumder, and A. Uppal, "Breast cancer diagnosis using N2 laser excited autofluorescence spectroscopy," *Lasers Surg. Med.* **21**(5), 417–422 (1997).
15. S. Majumder, P. Gupta, B. Jain, and A. Uppal, "UV excited autofluorescence spectroscopy of human breast tissues for discriminating cancerous tissue from benign tumor and normal tissue," *Lasers Life Sci.* **00**, 1–16 (1998).
16. I. Georgakoudi, B. C. Jacobson, M. G. Muller, E. E. Sheets, K. Badizadegan, D. L. Carr-Locke, C. P. Crum, C. W. Boone, R. R. Dasari, J. Van Dam, and M. S. Feld, "NAD(P)H and collagen as *in vivo* quantitative fluorescent biomarkers of epithelial precancerous changes," *Cancer Res.* **62**(3), 682–687 (2002).
17. G. Zonios, L. Perelman, V. Backman, R. Manoharan, M. Fitzmaurice, J. Crowe, R. R. Dasari, and M. Feld, "Diffuse reflectance spectroscopy of human adenomatous colon polyps *in vivo*," *Appl. Opt.*, **38**, 6628–6637 (1999).
18. J. W. Tunnell, A. E. Desjardins, L. Galindo, I. Georgakoudi, S. A. McGee, J. Mirkovic, M. G. Mueller, J. Nazemi, F. T. Nguyen, A. Wax, Q. Zhang, R. R. Dasari, and M. S. Feld, "Instrumentation for multi-modal spectroscopic diagnosis of epithelial dysplasia," *Technol. Cancer Res. Treat.* **2**(6), 505–514 (2003).
19. Z. Volynskaya, "Multi-modal spectroscopy of breast tissue," MS Thesis, MIT, p. 67 (2005).
20. J. M. Schmitt and G. Kumar, "Optical scattering properties of soft tissue: a discrete particle model," *Appl. Opt.* **37**(13), 2788–2798 (1998).



21. Y. Yang, E. J. Celmer, J. A. Koutcher, and R. R. Alfano, "DNA and protein changes caused by disease in human breast tissues probed by the Kubelka-Munk spectral functional," *Photochem. Photobiol.* **75**(6), 627–632 (2002).
22. H. J. van Staveren, C. J. M. Moes, J. van Marle, S. A. Prahl, and J. C. van Gemert, "Light scattering in intralipid-10% in the wavelength range of 400–1100 nm," *Appl. Opt.* **30**(31), 4507–4514 (1991).
23. M. Mueller, I. Georgakoudi, Q. Zhang, J. Wu, and M. S. Feld, "Intrinsic fluorescence spectroscopy in turbid media: disentangling effects of scattering and absorption," *Appl. Opt.* **40**(25), 4633–4646 (2001).
24. K. Shafer-Peltier, "Chemical basis for breast cancer diagnosis using raman spectroscopy," PhD Diss. MIT, 145 (2001).
25. S. Navea, A. de Juan, and R. Tauler, "Detection and resolution of intermediate species in protein folding processes using fluorescence and circular dichroism spectroscopies and multivariate curve resolution," *Anal. Chem.* **74**(23), 6031–6039 (2002).
26. R. Richards-Kortum and E. Sevick-Muraca, "Quantitative optical spectroscopy for tissue diagnosis," *Annu. Rev. Phys. Chem.* **47**, 555–606 (1996).
27. M. Fitzmaurice, "Principles and pitfalls of diagnostic test development: implications for spectroscopic tissue diagnosis," *J. Biomed. Opt.* **5**(2), 119–130 (2000).
28. G. M. Palmer, C. Zhu, T. M. Breslin, F. Xu, K. W. Gilchrist, and N. Ramanujam, "Comparison of multiexcitation fluorescence and diffuse reflectance spectroscopy for the diagnosis of breast cancer (March 2003)," *IEEE Trans. Biomed. Eng.* **50**(11), 1233–1242 (2003).
29. S. Kauppila, F. Stenback, J. Risteli, A. Jukkola, and L. Risteli, "Aberrant type I and type III collagen gene expression in human breast cancer in vivo," *J. Pathol.* **186**(3), 262–268 (1998).
30. S. H. Barsky, C. N. Rao, G. R. Grotendorst, and L. A. Liotta, "Increased content of Type V collagen in desmoplasia of human breast carcinoma," *Am. J. Pathol.* **108**(3), 276–283 (1982).
31. A. S. Haka, Z. Volynskaya, J. A. Gardecki, J. Nazemi, R. Shenk, N. Wang, R. R. Dasari, and M. S. Feld, "Diagnosing breast cancer using raman spectroscopy: prospective analysis," in preparation.